

Abstract

A new method is presented in this paper which analyses the scattered light of individual aerosol particles simultaneously at two different wavelengths in order to retrieve information on the particle type. We show that dust-like particles, such as volcanic ash, can be unambiguously discriminated from water droplets on a single particle level. As a future application of this method, the detection of volcanic ash particles should be possible in a humid atmosphere in the presence of cloud droplets. We show an example, how the characteristic behaviour of pure water's refractive index can be used to separate water droplets and dust-like particles which are commonly found in the micrometer size-range in the ambient air. The low real part of the water's refractive index around 2700–2800 nm results in low scattered light intensities compared to e.g. the visible wavelength range and this feature can be used for the particle identification.

The two-wavelength measurement setup was theoretically and experimentally tested and studied. Theoretical calculations were done using Mie theory. Comparing the ratio of the scattered light at the two wavelengths (R value) for water droplets and different dust types (basalt, andesite, African mineral dust, sand, volcanic ash, pumice) showed at least 9 times higher values (on average 70 times) for water droplets than for the dust types at any diameter within the particle size range of 2–20 μm . The envisaged measurement setup was built up into a laboratory prototype and was tested with different types of aerosols. We generated aerosols from the following powders simulating dust-like particles: cement dust, ISO 12103-1 A1 Ultrafine Test Dust and Ash from the 2012 eruption of the Etna volcano. Our measurements verified the theoretical considerations, the median experimental R value is 8–21 times higher for water than for the “dust” particles.

AMTD

8, 8701–8726, 2015

Dual-wavelength volcanic ash detector

Z. Jurányi et al.

Title Page

Abstract

Introduction

Conclusions

References

Tables

Figures



Back

Close

Full Screen / Esc

Printer-friendly Version

Interactive Discussion



1 Introduction

Atmospheric aerosol particles absorb and scatter solar radiation and, therefore, have an effect on the Earth's radiative budget and influence our climate. To understand and be able to estimate this effect, the physical and chemical properties of the atmospheric aerosols such as e.g. number concentration, number size distribution, chemical composition, optical properties and hygroscopicity have to be better understood and determined.

Aerosol particles, illuminated by light, interact with the electromagnetic radiation and scatter light in all directions. The intensity of the scattered light in a certain direction depends on the particle's size, refractive index, shape, scattering angle and the wavelength of the incident light. The scattering behaviour of a homogeneously mixed, spherical particle can be described by Mie theory (Bohren and Huffman, 2004). It needs the wavelength of the incident light, the scattering angle, the refractive index of particle relative to the carrier medium (in our case it is air) and the particle's diameter as input and provides an exact solution of the differential scattering cross section. The differential cross section as a function of the particle diameter show a distinct pattern with a rapidly fluctuating structure called Mie oscillations in the range where the particle diameter is comparable to the wavelength of the incident light.

The method of analysing scattered light from aerosol particles is a widely used aerosol measurement technique, which is mainly used for particle sizing and counting. Optical particle counters (OPC) collect scattered light from individual particles in a defined scattering angle range in order to gain information about the optical and/or physical properties of particles (e.g., Rosen, 1964; Binnig et al., 2007). These instruments are used to characterize aerosol particles since the 1940's (Kerker, 1997). The information on the scattered light intensity can be used to derive information on the size of the individual particles under certain assumptions regarding their refractive index and shape (Dick et al., 1994). For a well-defined observation volume, the frequency

AMTD

8, 8701–8726, 2015

Dual-wavelength volcanic ash detector

Z. Jurányi et al.

Title Page

Abstract

Introduction

Conclusions

References

Tables

Figures



Back

Close

Full Screen / Esc

Printer-friendly Version

Interactive Discussion



of encountered light pulses is used to derive the particle concentration and with the measured size the aerosol number size distribution can be inferred.

However, as it was already mentioned before, the light scattering is also dependent on the chemical composition of the aerosol particles through the refractive index of the particles. Therefore it is also possible to retrieve limited information on the chemical composition by measuring light scattering. Szymanski et al. (2002) and Nagy et al. (2007) have developed and investigated a dual-wavelength optical spectrometer. This instrument works with two laser sources at 532 and 685 nm wavelengths and four detectors collecting scattered light in forward and backward angular ranges. As a result, a set of four independently measured values from a detected particle allows the assessment of particle size and its complex refractive index.

In this paper, we introduce a method where also two monochromatic light sources are used and backscattered light is measured over a defined angular range for each wavelength. By selecting the correct specific wavelengths and detection angles, the ratio of the scattered light intensities can be used for component specific particle differentiation. The new approach is to select one wavelength such that a particular optical property of a certain particle type can be used for the envisaged particle differentiation. In our application, the specific optical characteristics of water in the infrared (IR) wavelength range is used to distinguish water droplet from dust particles such as volcanic ash.

Volcanic ash aerosol might be present in the atmosphere if emitted through volcanic eruptions. If the eruption is strong enough the volcanic ash cloud can reach altitudes of aviation and be a serious security risk to airplanes. It can severely damage jet engines and endanger passenger transportation (Casadevall, 1993). Such an event might therefore make it necessary to close down airports and airspaces. For example, the eruptions of the Eyjafjallajökull volcano in Iceland in April and May in 2010 resulted in partially closure of Europe's airspace for several days. The volcanic ash particles are usually found in the micrometer diameter range, e.g. after the eruption of the Eyjafjallajökull volcano, the measured volcanic ash volume size distribution had a mode

Dual-wavelength volcanic ash detector

Z. Jurányi et al.

Title Page

Abstract

Introduction

Conclusions

References

Tables

Figures



Back

Close

Full Screen / Esc

Printer-friendly Version

Interactive Discussion



around 3 μm (Bukowiecki et al., 2011) measured at the high-alpine research station Jungfrauoch, Switzerland.

Volcanic ash particles are not the only particles in the above mentioned micrometer size-range. Fortunately, the normal background dry aerosol mass concentration in the free troposphere is negligible (only a few $\mu\text{g m}^{-3}$, e.g. Cozic et al., 2008) when compared to the lower limit established for the area of low volcanic ash contamination (0.2 mg m^{-3}). In the presence of substantial water in the atmosphere the situation can be different; cloud droplets are also found in the supermicron size-range, and their mass/number concentration can easily reach the limit values established by the existing legislation for volcanic ash.

One optical method to distinguish between water droplets and volcanic ash particles is the measurement of the scattered light's polarisation ratio. Whether a particle is spherical or not can be detected using linear polarised incident light and detecting the polarisation state of the scattered light (Kobayashi et al., 2014). Spherical water droplets do not change the polarization state whereas non-spherical particles such as volcanic ash scatter the light depolarized (Munoz), which results in a decrease of the scattered light intensity in the original polarization plane and an increase in the perpendicular polarization plane. The back-scatter cloud probe (BCP) from droplet measurement technologies (Beswick et al., 2014) with the optional polarisation detection is a commercial instrument which uses this method.

Here we introduce a new method which is based on dual-wavelength scattered light measurement and able to distinguish between water droplets and other particles of dust origin.

2 Theory

The proposed component specific particle differentiation is based on the significant difference in the scattering behaviour of these components at least at one of the two wavelengths. This particular behaviour results in a significantly different value if the

Dual-wavelength volcanic ash detector

Z. Jurányi et al.

Title Page

Abstract

Introduction

Conclusions

References

Tables

Figures



Back

Close

Full Screen / Esc

Printer-friendly Version

Interactive Discussion



ratio of the scattered light intensity at the two different wavelengths is calculated (as a function of the particle diameter). The ratio R is defined as follows:

$$R(\lambda_1, \lambda_2, D) = \frac{dC(\Theta_1, D, m_1, \lambda_1)/d\Omega}{dC(\Theta_2, D, m_2, \lambda_2)/d\Omega} \quad (1)$$

where λ_1 and λ_2 are the selected wavelengths, $\frac{dC}{d\Omega}$ is the differential scattering cross section of the aerosol particle, m_1 and m_2 are the complex refractive indices of the aerosol particles at λ_1 and λ_2 , D is the diameter of the aerosol particle and Θ is the scattering angle. If the particles are spherical, $\frac{dC}{d\Omega}$ can be exactly calculated using the Mie theory (Bohren and Huffman, 2004). It can be experimentally determined as well as the ratio of the measured scattering signals at the two wavelengths.

With this, if the scattered light intensities of individual particles are measured simultaneously at both wavelengths, the particle differentiation will become possible because the ratio R depends on the particle chemical composition. If needed, the particles can not only be counted but also sized based on the scattered light's intensity at one of the wavelengths with the same method as traditional optical particle counters do. In the following we will show an application of this method which intends to separate water droplets from "dust" particles. Under "dust" particles, we understand aerosol particles in the μm size range of various origins: different kinds of mineral dust, road dust or particularly volcanic ash. For the particle differentiation, we use the unique optical behaviour of water and the same time we assume the lack of the same in the case of the dust particles. In order to demonstrate the selectivity, we compare the R ratios of water at these two wavelengths with that of several dusts.

Figure 1 shows the real and imaginary part of the water droplets' refractive index as a function of the wavelength of light (Rothman et al., 2013). The distinct absorption of water at $\lambda = 3 \mu\text{m}$ is seen in an elevated imaginary part of the refractive index and consequently in a distinct change in the real part. We use this behaviour to get a significantly different scattering behaviour of water compared to other aerosol components which might be present in the ambient air. For the experimental setup we have chosen

Dual-wavelength volcanic ash detector

Z. Jurányi et al.

Title Page

Abstract

Introduction

Conclusions

References

Tables

Figures



Back

Close

Full Screen / Esc

Printer-friendly Version

Interactive Discussion



$\lambda_1 = 660$ nm in the visible wavelength range and $\lambda_1 = 2750$ nm in the IR as a wavelength combination where water has significantly different refractive indices (see the grey dashed lines in Fig. 1).

In Table 1 we have summarized the refractive indices of water and several “dust like” aerosols at the two selected wavelengths. We used these literature values to calculate the R ratios and to simulate the performance of a dust/water specific optical particle counter. Water has significantly different refractive index values at λ_1 and λ_2 whereas the same for the dust-like components are not changing significantly between the selected wavelengths.

The differential cross section of the particles was calculated using a custom written Mie code assuming unpolarised incident light. Figure 2 shows the modelled scattered light intensity ratio R for water and “dust” particles as a function of the particle’s diameter in the 2–20 μm size range. $R(\lambda_1, \lambda_2, D)$ is calculated following Eq. (1), averaging the differential cross sections over the scattering angle ranges of 130–150 and 140–160° which simulates the employed optical measurement system with a non-zero detector opening. We have chosen to detect the backscattered light because the envisaged instrument application in the field aims at ambient stationary and aircraft deployed measurements. The low real part of the refractive index of water at 2750 nm compared to 660 nm is reflected by high $R(\lambda_1, \lambda_2, D)$ values with an average of ~ 70 compared to an average R of ~ 0.15 – 0.9 for different dust types. The band of the different ratio values of water (light blue shading in Fig. 2) and dust particles (light orange shading in Fig. 2) are well separated at any particle diameter of our interest, the diameter where R values are the least separated is around 2.5 μm , but even here, there is approximately a factor of 9 between water and dust.

As mentioned before, we used Mie calculation to model the scattered light from dust particles which assumes homogeneously composed particles with a spherical shape. However, dust particles are often non-spherical (e.g. Coz et al., 2010) and, therefore, their light scattering properties can differ from the values that are calculated using the Mie-theory. Curtis et al. (2008) studied the light scattering properties of many rep-

Dual-wavelength volcanic ash detector

Z. Jurányi et al.

Title Page

Abstract

Introduction

Conclusions

References

Tables

Figures



Back

Close

Full Screen / Esc

Printer-friendly Version

Interactive Discussion



**Dual-wavelength
volcanic ash detector**

Z. Jurányi et al.

Title Page

Abstract

Introduction

Conclusions

References

Tables

Figures



Back

Close

Full Screen / Esc

Printer-friendly Version

Interactive Discussion



representative dust aerosol components and found that a significant deviation between Mie-theory calculation and measurement exists. Especially for non-clay minerals, Mie calculations overestimate the backscattering signal up to a factor of two in the angle range of our interest (130–160°). Next to this, our knowledge of the refractive indices of the different dust-like components (Petzold et al., 2011, and references therein) are still quite uncertain, the literature values of the imaginary part of the complex refractive index varies between $< 1 \times 10^{-3}$ to 0.01 at a wavelength of 550 nm for mineral dust particles. However, as we see from Fig. 2 even if we underestimate the scattering signal ratios by multiple factors, the R values for water and dust particles will be still different enough to have the possibility of a proper differentiation.

3 Experimental

To verify the theoretical results we built an experimental setup to generate dust and water particles and a system for the two-wavelength light scattering measurement.

3.1 Particle generation

During the experiments, we used two different methods for aerosol generation. The powder-based samples were brought into the aerosol phase with the help of a small scale powder disperser (SSPD, TSI 3344). The powder was distributed on a round table which turns with a controllable speed below a capillary tube with a venturi aspirator. Particles are sucked up from the turntable by the low pressure that is caused by the high air velocity in a venturi tube and transmitted further by the air flow. The aerosol exits the SSPD with 5–20 dm³ min⁻¹ flow-rate, the particle concentration can be varied by placing more or less powder on the turntable and/or by changing its angular velocity.

The water droplets were generated by a nebulizer, filled with tap water as the particle source. The generated droplets were injected into a humidified (RH > 90 %) airstream with 5 dm³ min⁻¹ flow-rate in order to accelerate and transport the droplets to either

the size distribution or the optical measurement. The length of the transport tubes was as short as possible (< 20 cm) in order to minimize the evaporation losses and the shrinking of the droplets.

3.2 Size distribution measurements

The particle number size distribution was measured with an aerodynamic particle sizer (APS, TSI 3321) in the aerodynamic diameter range of $0.7\text{--}20\ \mu\text{m}$. This instrument sizes the aerosol particles by measuring the time-of-flight of the individual particles in an accelerating flow field. The total flow-rate of the APS was $5\ \text{dm}^3\ \text{min}^{-1}$ with $1\ \text{dm}^3\ \text{min}^{-1}$ aerosol flow rate.

3.3 Optical measurement setup

Based on the theoretical calculations, a laboratory optical measurement setup was realized to test our theoretical considerations. The experimental setup (an illustration is shown in Fig. 2) is an “open setup” where ambient light can reach the detectors. It was built on an optical table of $60\ \text{cm} \times 60\ \text{cm}$. The visible light source is a $660\ \text{nm}$ laser diode with collimation optics, the power of this laser was set that the incident visible light power reached values of $\sim 20\ \text{mW}$ at the particle detection volume during the measurements. This power was checked manually before and after each experiment with a power meter.

The IR laser is a semiconductor disk laser module, operating at $2750\ \text{nm}$ wavelength, and has a maximal power of $\sim 90\ \text{mW}$. The laser was developed at the Fraunhofer Institute for Applied Solid State Physics in Freiburg, Germany (IAF). The power of this laser was also checked before and after each experiment. The IR radiation is collimated with BaF_2 lenses.

Both collimated laser beams are directed to a common detection volume of $\sim 1\text{--}3\ \text{mm}^3$. The beam adjustment is achieved by mirrors (gold for the IR and silver for the visible laser) held by tiltable and rotatable precision mirror mounts.

Dual-wavelength volcanic ash detector

Z. Jurányi et al.

Title Page

Abstract

Introduction

Conclusions

References

Tables

Figures

◀

▶

◀

▶

Back

Close

Full Screen / Esc

Printer-friendly Version

Interactive Discussion



**Dual-wavelength
volcanic ash detector**

Z. Jurányi et al.

Title Page

Abstract

Introduction

Conclusions

References

Tables

Figures



Back

Close

Full Screen / Esc

Printer-friendly Version

Interactive Discussion



The scattered visible light is detected by a Hamamatsu photomultiplier (H7711-04) under 140° central scattering angle with $\sim \pm 3^\circ$ opening angle. Due to the relative large size and asymmetric form of the sensitive detector area ($4\text{ mm} \times 20\text{ mm}$) an iris with 0.8 mm hole diameter was placed between a lens (N-BK7 bi-convex, 12.7 mm diameter, 20 mm focal length) and the detector to strictly limit the detection angle. This ensures that predominately the light scattered by the particles in the joint illuminated volume is detected. To minimize the detected background light, a bandpass filter (660 nm middle wavelength and 10 nm full width at half maximum) was placed in front of the visible detector.

In the visible wavelength affordable, commercial photodetectors exist (photomultipliers, avalanche photodiodes), that are able to detect as low light levels as a single photon. Unfortunately, such a technique is not yet commercially available in the IR range. The scattered IR light was measured by a VIGO PV-4TE photovoltaic IR detector under 150° central scattering angle ($\pm 10^\circ$), optimized to measure at $\sim 3\text{ }\mu\text{m}$ wavelength. This detector has a built-in 4-stage thermoelectric cooler, which cools down the detector to 195 K in order to reduce the detector's noise and increase its responsivity. The detector module has a $100\text{ Hz} - 1\text{ MHz}$ bandwidth. The collection and focusing optics included two bi-convex CaF_2 lenses with 12.7 and 25.4 mm diameters and 20 and 25.4 mm focal lengths, respectively. A bandpass filter was not used here because no significant IR background light could be encountered in the laboratory.

The measurement setup requires highly precise adjustment of both the lasers and detectors to have a joint detection volume which are imaged by both detectors. Therefore, both detectors were placed on pitch and yaw platforms with micrometer screws. The measured voltage signals from the detectors are digitized by a National Instruments PCI card (NI 5112) built in a PC. The voltage peaks resulting from particles flying through the instrument's detection volume were identified, sized and saved using custom-written LabVIEW software.

Data from the detectors were recorded with 1 MHz time resolution, and every second 10^6 data points per detectors were analysed. The voltage peaks caused by single

**Dual-wavelength
volcanic ash detector**Z. Jurányi et al.

Title Page

Abstract

Introduction

Conclusions

References

Tables

Figures



Back

Close

Full Screen / Esc

Printer-friendly Version

Interactive Discussion



particle scattering have to be separated from the detector noise. Therefore only peaks with maximal voltage values exceeding a certain threshold are considered. The baseline of the detectors can change with time, because e.g. the ambient light reaching the visible detector changes as well. This is the reason why we define a new peak threshold for every 1 s data series. It is assumed that the detector baselines remained constant within these 1 s measurement periods and was identified as the median of all the voltage values. Due to the setup and alignment of the two lasers and the detectors, the detection volumes are not entirely identical for both wavelengths. Therefore, some of the particles are only detected by one of the detectors but not by the other. We only considered the coincident events (i.e. the peaks that appear simultaneously in both detectors). In practice, it was achieved by selecting the peaks that are timely separated by less than half of a peak width. As mentioned below, concentrations were chosen such that the probability of two particles being at the same time in the detection volume is negligible.

Figure 4 illustrates our threshold selection. One second of detector background data was simulated with Gaussian noise around a median value of 0.05 V with a standard deviation of 0.01 V. These values were chosen to match the experienced real values the best. The histogram of the detector signal without aerosol particles passing by is shown as a solid green line in Fig. 4. The other coloured lines show the detector signal histograms if different number (blue: 1.5 %, purple: 4 %, orange: 10 % of the total data points containing data from a scattered light peak) of peaks were added to the background. Panel a of Fig. 4 shows a short segment of the data. The peaks are randomly distributed in time, having a Gaussian form with a standard deviation of 10 points (10 μ s). The peak amplitudes were chosen to be exponentially distributed with 1 V average and standard deviation. These parameters were chosen to simulate the obtained results well. Our aim was to define a threshold, based on the data points' histogram which is not significantly influenced by the number of the detectable peaks. As one can see in Fig. 4, the medians and the 75th percentiles (vertical coloured, solid lines) of the distributions are only slightly influenced by the number of added

**Dual-wavelength
volcanic ash detector**

Z. Jurányi et al.

Title Page

Abstract

Introduction

Conclusions

References

Tables

Figures



Back

Close

Full Screen / Esc

Printer-friendly Version

Interactive Discussion



peaks, whereas the 99th percentiles (vertical dotted lines) are highly. Therefore a high percentile value cannot be used as a threshold for identifying the particle peaks. We have defined the threshold as a constant factor C times the difference between the 75th percentile and the median added to the median value. These values are also shown in Fig. 4 as dashed, vertical lines. At the highest peak occurrence (10 % of the data points contain peak values) this threshold is 4 % higher than for the background case, whereas for the other two examples the difference is less than 2 %. For the optical experiments, the factor C was chosen to be 3.4. The peaks exceeding this threshold are identified as particle peaks, and sized. The position (time) and amplitude of each peak are saved as a text file for further data analysis.

4 Experimental results

During the laboratory measurements next to the water droplets the following dust powders were used to simulate a variety of different atmospheric dust types: cement dust (commercial Portland cement), ISO 12103-1 A1 Ultrafine Test Dust (Powder Technology Inc.) and Ash from the 2012 eruption of the Etna volcano. Particle number size distribution measurements were performed next to the optical measurements. Figure 5 shows these measured number size distributions of the different generated aerosols. The generated “dust” aerosol particles had 1.38, 1.41 and 1.58 μm mean aerodynamic diameter for Etna ash, ISO test dust, and cement, respectively. The water droplets were significantly larger in size with 3.45 μm mean diameter.

For each optical experiment 2×10^3 – 10^5 individual particles which generated coincident peaks in both detectors were measured. The particle concentration was low (less than ~ 200 particles s^{-1}) such that no coincidence artefacts were encountered. This means that on average less than 1 % of the data points contained particle generated peaks. The dust particle measurement were conducted with a flow rate of $20 \text{ dm}^3 \text{ min}^{-1}$ which correspond to an average air exit velocity of $\sim 30 \text{ ms}^{-1}$ and $\sim 50 \mu\text{s}$ average

peak width. The corresponding average peak width and flow-rate for the water droplet experiments were $\sim 200 \mu\text{s}$ at $5 \text{ dm}^3 \text{ min}^{-1}$, respectively.

The R ratio for individual particles was calculated by dividing the peak amplitude voltage measured by the visible detector by the same value measured by the IR detector.

This experimental R_{exp} value is not equal to the theoretical one, since the experimental setup was not calibrated for the different detector efficiencies, numerical apertures, incident laser intensities and optical losses. This is the reason why the experimental and the theoretically R values are connected by a constant factor, which does not depend on the measured particle type.

Even for monodisperse aerosol particles, many different R_{exp} values are expected because of the different orientation of the two lasers with Gaussian-like beam profiles: the two lasers are not entirely overlapping and therefore it must be expected that, for example, a particle crosses one laser close to its intensity maximum and the other laser at the border at lower intensities. As a consequence, a distribution of R values is encountered.

For this reason we do not evaluate the R ratios of the individual particles but rather interpret their probability distribution. Figure 6 shows these probability distributions, as measured for the different aerosol types. The solid lines show the probability density functions (left axis), the dashed lines show the cumulative density functions (right axis).

As we have expected from the theoretical considerations, the R values of water droplets are shifted to significant higher values (please note the logarithmic x axis of Fig. 6) compared to the R values of dust particles. The median R values for the different particle types are also shown in Table 2. We found that the median was 8–21 times higher for water than for the various dust types. With this, our hypothesis of a dual-wavelength light scattering instrument being able to differentiate between specific components is verified.

Table 2 also shows modelled R values that were calculated for water, ISO test dust and volcanic ash. Cement was not included in these calculations because we had no information about its refractive index at 2750 nm wavelength. The refractive index of

Dual-wavelength volcanic ash detector

Z. Jurányi et al.

Title Page

Abstract

Introduction

Conclusions

References

Tables

Figures



Back

Close

Full Screen / Esc

Printer-friendly Version

Interactive Discussion



**Dual-wavelength
volcanic ash detector**

Z. Jurányi et al.

Title Page

Abstract

Introduction

Conclusions

References

Tables

Figures

I◀

▶I

◀

▶

Back

Close

Full Screen / Esc

Printer-friendly Version

Interactive Discussion



ISO test dust was assumed to be equal to the value of African mineral dust in Table 1. The R value calculations also used the measured number size distributions as input and assumed a minimal detection limit of the optical system of either 1 or 2 μm particle diameter. The theoretical estimations of the R values cannot be directly compared to the measurement values because the optical measurement setup was not calibrated with respect to detector efficiencies, incident laser intensities, and optical transmissions. However, a comparison of the relative change in measured and modelled R values (water to dust R value ratio, last row of Table 2) is possible as these are not affected by the above-mentioned calibration coefficients. Measurements show that R values of water are a factor of 8–21 higher than for the dust particles. The calculated increase lies between a factor of 16–99 and is dependent on the component and on the smallest detectable particle size. We consider this as a reasonably good agreement bearing all the different uncertainties in mind, such as the ill-defined lower size cut (size of the smallest detectable particle), the non-sphericity of the dust aerosols, the different components considered during calculations and measurement, and the restricted knowledge on the refractive index of the different dust particles.

5 Conclusions

We have built and tested (theoretically and experimentally) a laboratory prototype of an aerosol measurement instrument, which is detecting backscattered light at two different wavelengths simultaneously from single particles at 660 and 2750 nm. This measurement setup aims successfully for the separation of water droplets and “dust” particles such as volcanic ash. We use the IR to visible scattered light intensity ratio (R value) as an indicator to decide if the detected particle is a water droplet or not. The low light scattering of water at 2750 nm compared to the visible range results in high R values for water droplets.

We modelled the R values for water droplets and different kind of dust particles (basalt, andesite, African mineral dust, sand, volcanic ash, pumice) using Mie theory

**Dual-wavelength
volcanic ash detector**

Z. Jurányi et al.

Title Page

Abstract

Introduction

Conclusions

References

Tables

Figures



Back

Close

Full Screen / Esc

Printer-friendly Version

Interactive Discussion



in the particle size range of 2–20 μm and found as we expected that at any size the R ratios of water are factors higher (on average 70) than the ones for the dust types. We have also built up a laboratory measurement setup to test practically our method. With the current experimental setup, we were only able to compare statistically the visible to IR scattering ratios since particles were experiencing different incident laser intensities due to the Gaussian laser beam profiles. We have shown that the experimental median R value is 8–21 times higher for water than for the various aerosol types we used for dust simulation (cement, ISO test dust and volcanic ash).

In the future, the measurement setup will be modified such that the problem originating from the incident light intensity's inhomogeneity will be minimized. Combining the two laser beams having the same beam diameter with a dichroic mirror and/or applying an inversion algorithm Beswick et al. (2014) are possible solutions. This is necessary in order to make the single particle sizing possible. For this reason, the size dependence of the single particle scattering at the visible wavelength can be used. A new prototype of the instrument will be developed which is deployable for stationary, ambient measurement and on aircrafts as well. During these ambient tests, the measurement setup will not only be tested for the separation of water droplets and dust particles but also for the distinction of ice crystals. Our theoretical calculations show that with a slightly different IR wavelength of 2790 nm a discrimination of dust and ice crystals should also be possible.

Acknowledgements. This work was supported by the Swiss Federal Office of Civil Aviation. We would like to thank the Fraunhofer Institute for Applied Solid State Physics, Freiburg, Germany for providing the IR laser for the experiments. We thank Martin Ebert (Technical University Darmstadt) for the Etna ash sample. Erik Hermann (Paul Scherrer Institut) is acknowledged for providing the APS and Günther Wehrle (Paul Scherrer Institut) for the fruitful discussions.

References

- Beswick, K., Baumgardner, D., Gallagher, M., Volz-Thomas, A., Nedelec, P., Wang, K.-Y., and Lance, S.: The backscatter cloud probe – a compact low-profile autonomous optical spectrometer, *Atmos. Meas. Tech.*, 7, 1443–1457, doi:10.5194/amt-7-1443-2014, 2014. 8705, 8715
- Binnig, J., Meyer, J., and Kasper, G.: Calibration of an optical particle counter to provide mass for well-defined particle materials, *J. Aerosol Sci.*, 38, 325–332, doi:10.1016/j.jaerosci.2006.12.001, 2007. 8703
- Bohren, C. and Huffman, D.: *Absorption and Scattering of Light by Small Particles*, Wiley-VCH, Weinheim, Germany, 2004. 8703, 8706
- Bukowiecki, N., Zieger, P., Weingartner, E., Jurányi, Z., Gysel, M., Neininger, B., Schneider, B., Hueglin, C., Ulrich, A., Wichser, A., Henne, S., Brunner, D., Kaegi, R., Schwikowski, M., Tobler, L., Wienhold, F. G., Engel, I., Buchmann, B., Peter, T., and Baltensperger, U.: Ground-based and airborne in-situ measurements of the Eyjafjallajökull volcanic aerosol plume in Switzerland in spring 2010, *Atmos. Chem. Phys.*, 11, 10011–10030, doi:10.5194/acp-11-10011-2011, 2011. 8705
- Casadevall, T. J.: Volcanic hazards and aviation safety, lessons of the past decade, *FAA Aviation Safety Journal*, 2, 9–17, 1993. 8704
- Coz, E., Gómez-Moreno, F. J., Casuccio, G. S., and Artíñano, B. N.: Variations on morphology and elemental composition of mineral dust particles from local, regional, and long-range transport meteorological scenarios, *J. Geophys. Res-Atmos.*, 115, D12204, doi:10.1029/2009JD012796, 2010. 8707
- Cozic, J., Verheggen, B., Weingartner, E., Crosier, J., Bower, K. N., Flynn, M., Coe, H., Henning, S., Steinbacher, M., Henne, S., Collaud Coen, M., Petzold, A., and Baltensperger, U.: Chemical composition of free tropospheric aerosol for PM1 and coarse mode at the high alpine site Jungfraujoch, *Atmos. Chem. Phys.*, 8, 407–423, doi:10.5194/acp-8-407-2008, 2008. 8705
- Curtis, D. B., Meland, B., Aycibin, M., Arnold, N. P., Grassian, V. H., Young, M. A., and Kleiber, P. D.: A laboratory investigation of light scattering from representative components of mineral dust aerosol at a wavelength of 550 nm, *J. Geophys. Res-Atmos.*, 113, D08210, doi:10.1029/2007JD009387, 2008. 8707

AMTD

8, 8701–8726, 2015

Dual-wavelength volcanic ash detector

Z. Jurányi et al.

Title Page

Abstract

Introduction

Conclusions

References

Tables

Figures



Back

Close

Full Screen / Esc

Printer-friendly Version

Interactive Discussion



**Dual-wavelength
volcanic ash detector**

Z. Jurányi et al.

Title Page

Abstract

Introduction

Conclusions

References

Tables

Figures

◀

▶

◀

▶

Back

Close

Full Screen / Esc

Printer-friendly Version

Interactive Discussion



- Di Biagio, C., Boucher, H., Caquineau, S., Chevaillier, S., Cuesta, J., and Formenti, P.: Variability of the infrared complex refractive index of African mineral dust: experimental estimation and implications for radiative transfer and satellite remote sensing, *Atmos. Chem. Phys.*, 14, 11093–11116, doi:10.5194/acp-14-11093-2014, 2014. 8719
- 5 Dick, W. D., McMurry, P. H., and Bottiger, J. R.: Size and composition-dependent response of the DAWN – a multiangle single-particle optical detector, *Aerosol Sci. Tech.*, 20, 345–362, doi:10.1080/02786829408959690, 1994. 8703
- Grainger, R. G., Peters, D. M., Thomas, G. E., Smith, A. J. A., Siddans, R., Carboni, E., and Dudhia, A.: Measuring volcanic plume and ash properties from space, *Geol. Soc. SP*, 380, 293–320, doi:10.1144/SP380.7, 2013. 8719
- 10 Kerker, M.: Light scattering instrumentation for aerosol studies: an historical overview, *Aerosol Sci. Tech.*, 38, 522–540, doi:10.1080/02786829708965492, 1997. 8703
- Kobayashi, H., Hayashi, M., Shiraiishi, K., Nakura, Y., Enomoto, T., Miura, K., Takahashi, H., Igarashi, Y., Naoe, H., Kaneyasu, N., Nishizawa, T., and Sugimoto, N.: Development of a polarization optical particle counter capable of aerosol type classification, *Atmos. Environ.*, 15 97, 486–492, doi:10.1016/j.atmosenv.2014.05.006, 2014. 8705
- Koepke, P., Hess, M., Schult, I., and Shettle, E. P.: Global Aerosol Data Set, Report No. 243, Max-Planck-Institut für Meteorologie, Hamburg, Germany, p. 37, 1997. 8719
- Nagy, A., Szymanski, W., Gál, P., Golczewski, A., and Czitrovsky, A.: Numerical and experimental study of the performance of the dual wavelength optical particle spectrometer (DWOPS), *J. Aerosol Sci.*, 38, 467–478, doi:10.1016/j.jaerosci.2007.02.005, 2007. 8704
- Petzold, A., Rasp, K., Weinzierl, B., Esselborn, M., Hamburger, T., Dörnbrack, A., Kandler, K., Schütz, L., Knippertz, P., Fiebig, M., and Virkkula, A.: Saharan dust absorption and refractive index from aircraft-based observations during SAMUM 2006, *Tellus B*, 61, 25 doi:10.1111/j.1600-0889.2008.00383.x, 2011. 8708, 8719
- Pollack, J. B., Toon, O. B., and Khare, B. N.: Optical properties of some terrestrial rocks and glasses, *Icarus*, 19, 372–389, doi:10.1016/0019-1035(73)90115-2, 1973. 8719
- Rosen, J. M.: The vertical distribution of dust to 30 Kilometers, *J. Geophys. Res.*, 69, 4673–4676, 1964. 8703
- 30 Rothman, L., Gordon, I., Babikov, Y., Barbe, A., Benner, D. C., Bernath, P., Birk, M., Biz-zocchi, L., Boudon, V., Brown, L., Campargue, A., Chance, K., Cohen, E., Coudert, L., Devi, V., Drouin, B., Fayt, A., Flaud, J.-M., Gamache, R., Harrison, J., Hartmann, J.-M., Hill, C., Hodges, J., Jacquemart, D., Jolly, A., Lamouroux, J., Roy, R. L., Li, G.,

Long, D., Lyulin, O., Mackie, C., Massie, S., Mikhailenko, S., Müller, H., Naumenko, O., Nikitin, A., Orphal, J., Perevalov, V., Perrin, A., Polovtseva, E., Richard, C., Smith, M., Starikova, E., Sung, K., Tashkun, S., Tennyson, J., Toon, G., Tyuterev, V., and Wagner, G.: The HITRAN2012 molecular spectroscopic database, *J. Quant. Spectrosc. Ra.*, 130, 4–50, doi:10.1016/j.jqsrt.2013.07.002, 2013. 8706, 8719, 8721

5 Szymanski, W. W., Nagy, A., Czitrovszky, A., and Jani, P.: A new method for the simultaneous measurement of aerosol particle size, complex refractive index and particle density, *Meas. Sci. Technol.*, 13, 303–307, doi:10.1088/0957-0233/13/3/311, 2002. 8704

10 Volz, F. E.: Infrared optical constants of ammonium sulfate, Sahara dust, volcanic pumice, and flyash, *Appl. Optics*, 12, 564–568, doi:10.1364/AO.12.000564, 1973. 8719

AMTD

8, 8701–8726, 2015

Dual-wavelength volcanic ash detector

Z. Jurányi et al.

Title Page

Abstract

Introduction

Conclusions

References

Tables

Figures



Back

Close

Full Screen / Esc

Printer-friendly Version

Interactive Discussion



Dual-wavelength volcanic ash detector

Z. Jurányi et al.

Table 1. The refractive index of water and different dust types at 660 and 2750 nm wavelength.

Aerosol Type	Refractive Index at 660 nm [-]	Refractive index at 2750 nm [-]	Reference
Water Droplets	$1.33 + 1.9 \times 10^{-8}i$	$1.14 + 5.9 \times 10^{-2}i$	Rothman et al. (2013)
Basalt	$1.52 + 1.1 \times 10^{-3}i$	$1.50 + 3.5 \times 10^{-3}i$	Pollack et al. (1973)
Andesite	$1.47 + 1.6 \times 10^{-3}i$	$1.46 + 5.0 \times 10^{-3}i$	Pollack et al. (1973)
African Mineral Dust	$1.55 + 3.0 \times 10^{-4}i$ at 700 nm	$1.50 + 1.0 \times 10^{-2}i$	Di Biagio et al. (2014) Petzold et al. (2011)
Sand	$1.53 + 4.5 \times 10^{-3}i$	$1.52 + 2.7 \times 10^{-2}i$	Koepke et al. (1997)
Volcanic Ash	$1.57 + 0i$	$1.51 + 3.6 \times 10^{-2}i$	Grainger et al. (2013)
Pumice	$1.46 + 1 \times 10^{-2}i$	$1.50 + 8.0 \times 10^{-3}i$	Volz (1973)

Title Page

Abstract

Introduction

Conclusions

References

Tables

Figures

I◀

▶I

◀

▶

Back

Close

Full Screen / Esc

Printer-friendly Version

Interactive Discussion



Dual-wavelength volcanic ash detector

Z. Jurányi et al.

Title Page

Abstract

Introduction

Conclusions

References

Tables

Figures

◀

▶

◀

▶

Back

Close

Full Screen / Esc

Printer-friendly Version

Interactive Discussion



Table 2. Median experimental and theoretical R values for water and some dust types.

Aerosol Type	Median of the R value		
	Experimental	Theoretical, $D > 1 \mu\text{m}$	Theoretical, $D > 2 \mu\text{m}$
Cement dust	15	–	–
ISO test dust	17	3.2	0.6
Etna volcanic ash	41	3.8	1.0
Water droplets	308	59.2	58.9
Water to dust ratio	8–21	16–19	60–99

**Dual-wavelength
volcanic ash detector**

Z. Jurányi et al.

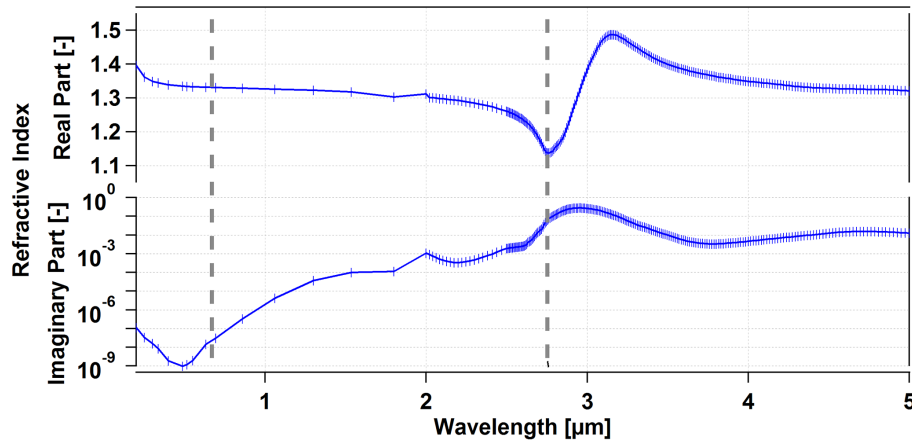


Figure 1. Real and imaginary part of the refractive index of water as a function of wavelength (Rothman et al., 2013), the dashed grey lines show our two selected wavelengths of 660 and 2750 nm.

[Title Page](#)[Abstract](#)[Introduction](#)[Conclusions](#)[References](#)[Tables](#)[Figures](#)[◀](#)[▶](#)[◀](#)[▶](#)[Back](#)[Close](#)[Full Screen / Esc](#)[Printer-friendly Version](#)[Interactive Discussion](#)

Dual-wavelength
volcanic ash detector

Z. Jurányi et al.

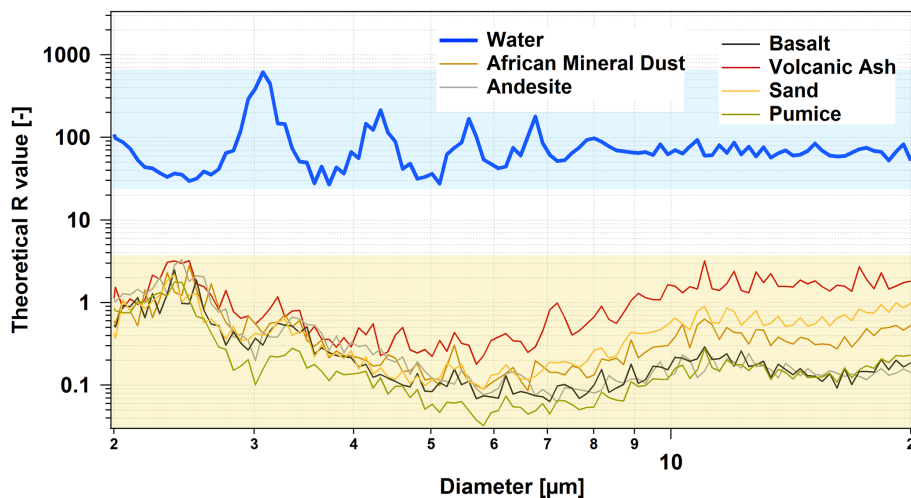


Figure 2. The theoretical R values at $\lambda_1 = 660$ nm and $\lambda_2 = 2750$ nm as a function of the particle diameter for different types of aerosols.

[Title Page](#)[Abstract](#)[Introduction](#)[Conclusions](#)[References](#)[Tables](#)[Figures](#)[◀](#)[▶](#)[◀](#)[▶](#)[Back](#)[Close](#)[Full Screen / Esc](#)[Printer-friendly Version](#)[Interactive Discussion](#)

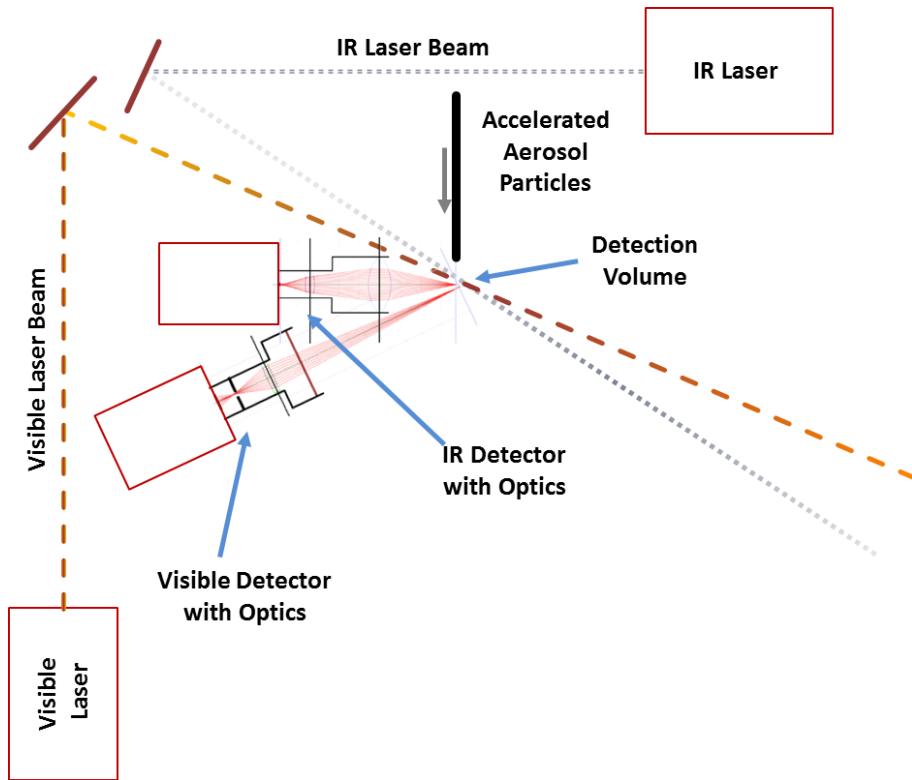


Figure 3. Drawing of the dual-wavelength optical measurement setup.

Title Page	
Abstract	Introduction
Conclusions	References
Tables	Figures
◀	▶
◀	▶
Back	Close
Full Screen / Esc	
Printer-friendly Version	
Interactive Discussion	



**Dual-wavelength
volcanic ash detector**

Z. Jurányi et al.

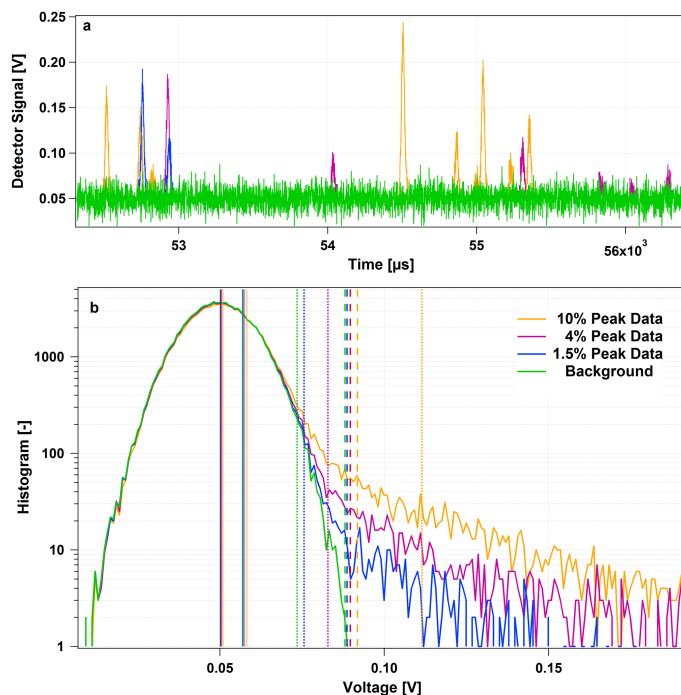


Figure 4. Simulated detector signal data without (green lines) and with different number of particle peaks (blue, purple and orange lines). Panel (a) shows a short segment of the simulated data whereas panel (b) shows the histograms of the data points on a logarithmic scale as a function of the detector voltage signal. See the text for details on the meaning of the vertical lines.

[Title Page](#)[Abstract](#)[Introduction](#)[Conclusions](#)[References](#)[Tables](#)[Figures](#)[◀](#)[▶](#)[◀](#)[▶](#)[Back](#)[Close](#)[Full Screen / Esc](#)[Printer-friendly Version](#)[Interactive Discussion](#)

Dual-wavelength
volcanic ash detector

Z. Jurányi et al.

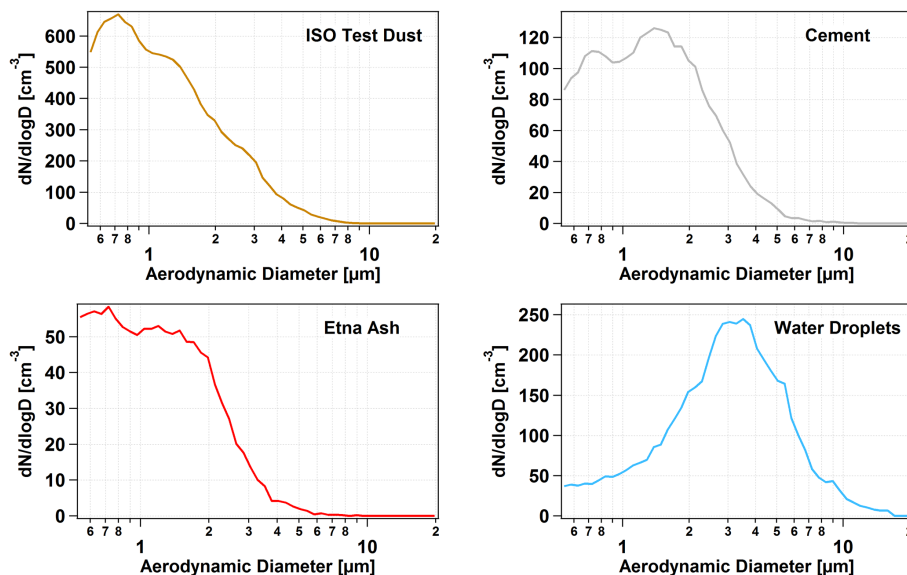


Figure 5. Typical number size distributions of the different aerosol types as a function of the aerodynamic particle diameter measured with an APS.

[Title Page](#)[Abstract](#)[Introduction](#)[Conclusions](#)[References](#)[Tables](#)[Figures](#)[◀](#)[▶](#)[◀](#)[▶](#)[Back](#)[Close](#)[Full Screen / Esc](#)[Printer-friendly Version](#)[Interactive Discussion](#)

Dual-wavelength
volcanic ash detector

Z. Jurányi et al.

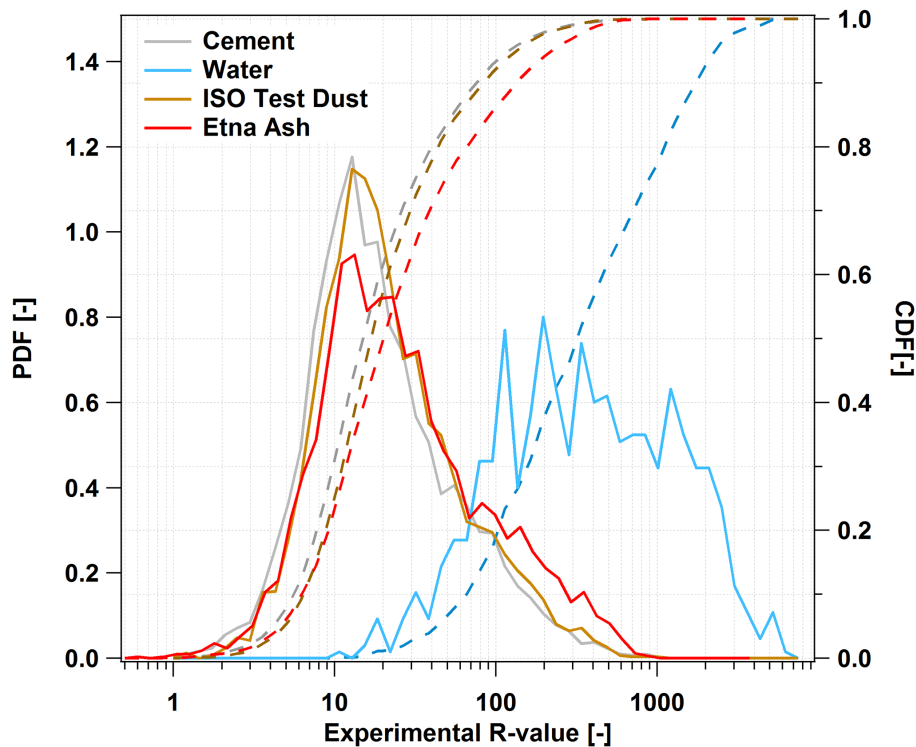


Figure 6. Measured probability density functions (left axis, solid lines) and cumulative density functions (right axis, dashed lines) of R values for water droplets and different dust-like aerosols.

[Title Page](#)[Abstract](#)[Introduction](#)[Conclusions](#)[References](#)[Tables](#)[Figures](#)[◀](#)[▶](#)[◀](#)[▶](#)[Back](#)[Close](#)[Full Screen / Esc](#)[Printer-friendly Version](#)[Interactive Discussion](#)